Thermofluids: Energy & Design

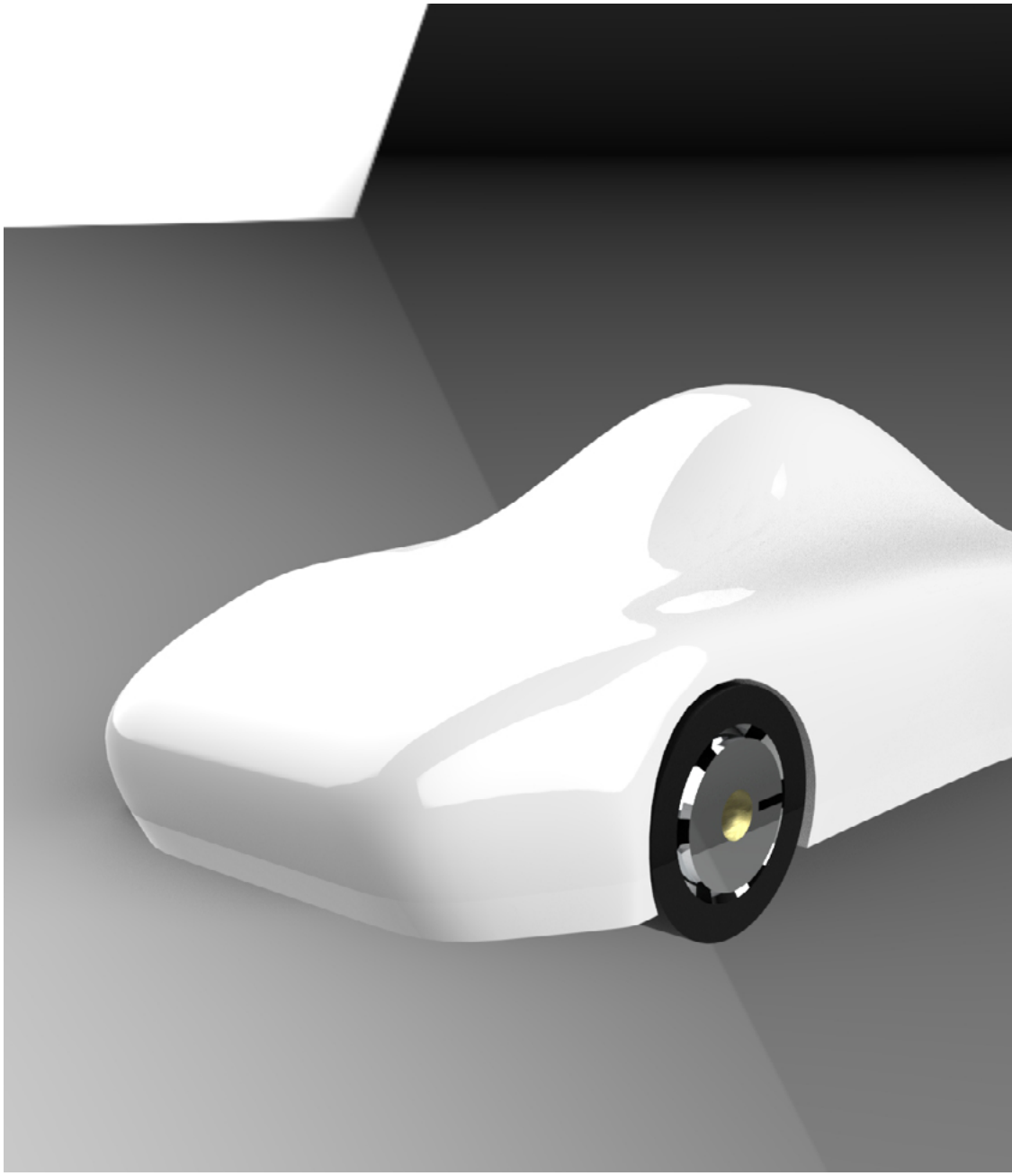

Vehicle Design Aerodynamics

Beam Suwiwatchai
02026376

Abstract

This paper achieved the final concept design by running CFD analysis on airflow pressure and velocity after carefully setting up the simulation environment using Solidworks Fluid Simulation Wizard. From the analysis, it was found that the initial design's drag coefficient was 36.6% higher than a contemporary sports car, with the main cause being the difference in size between the two vehicles. Overall, the revised concept design aims to reduce said drag by reducing vehicle size, reducing sharp edges, and adding rear diffuser.

Concept Design

Currently, there is a significant increase in global climate concerns amongst the public resulting in a notable technological and social push towards green energy and sustainability, particularly in the automotive industry where many manufacturers continue to deliver greater battery range and driving performance. With electric motors providing greater torque and snappier acceleration translating to a better experience for enthusiasts, there is a market currently unfulfilled by traditional automotive manufacturers: the **high-performance electric car**.

Vehicle Design Inspirations

When an electric vehicle comes to mind, many would think of a minimalistic and sleek design, which is the opposite of what many traditional car enthusiasts would expect from their idealistic car. Therefore, the main objective of this concept is to design a car which would appeal to **classic** motorsports enthusiasts while maintaining **futuristic eco-friendly** electric car characteristics.

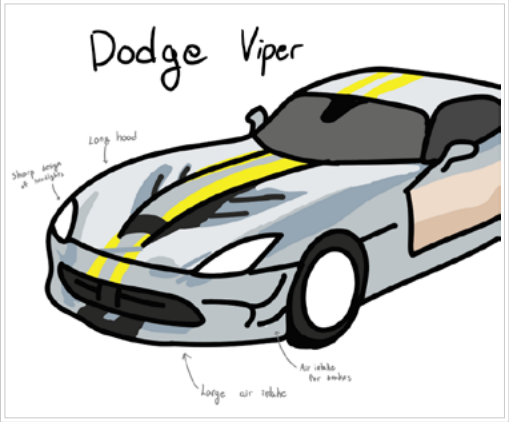

Muscle Car Body Characteristics
Muscle car market is one that is slow to change regarding electrifications, by increasing the body size to that of traditional muscle cars, the design hopes to provide greater driver comfort and trunk space for everyday usage.

Large Frontal Air-intake
The new design would incorporate many of the frontal bumper design of the Dodge viper with its air-intake systems for battery and brakes cooling.

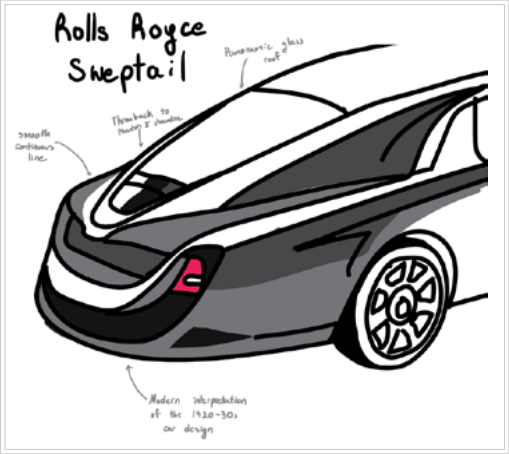

Sweptail
One of many notable characteristics of the 1930s era cars are its sweptail design, with converging lines at the rear of the vehicle.

Fastback Design
One of many characteristics present in high-performance car is the fastback body design with continuous line from the front to back resulting in less drag.

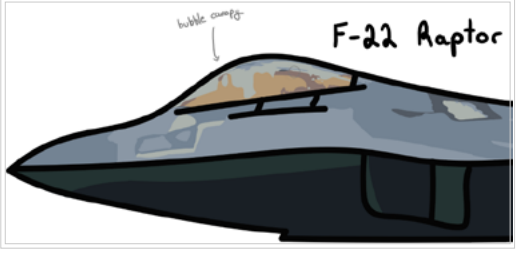

Panoramic Bubble Cabin
To increase visibility and driving experience, the design would include panoramic passenger cabin similar to those of fighter jets to allow greater connection between the driver, the car, and the environment.

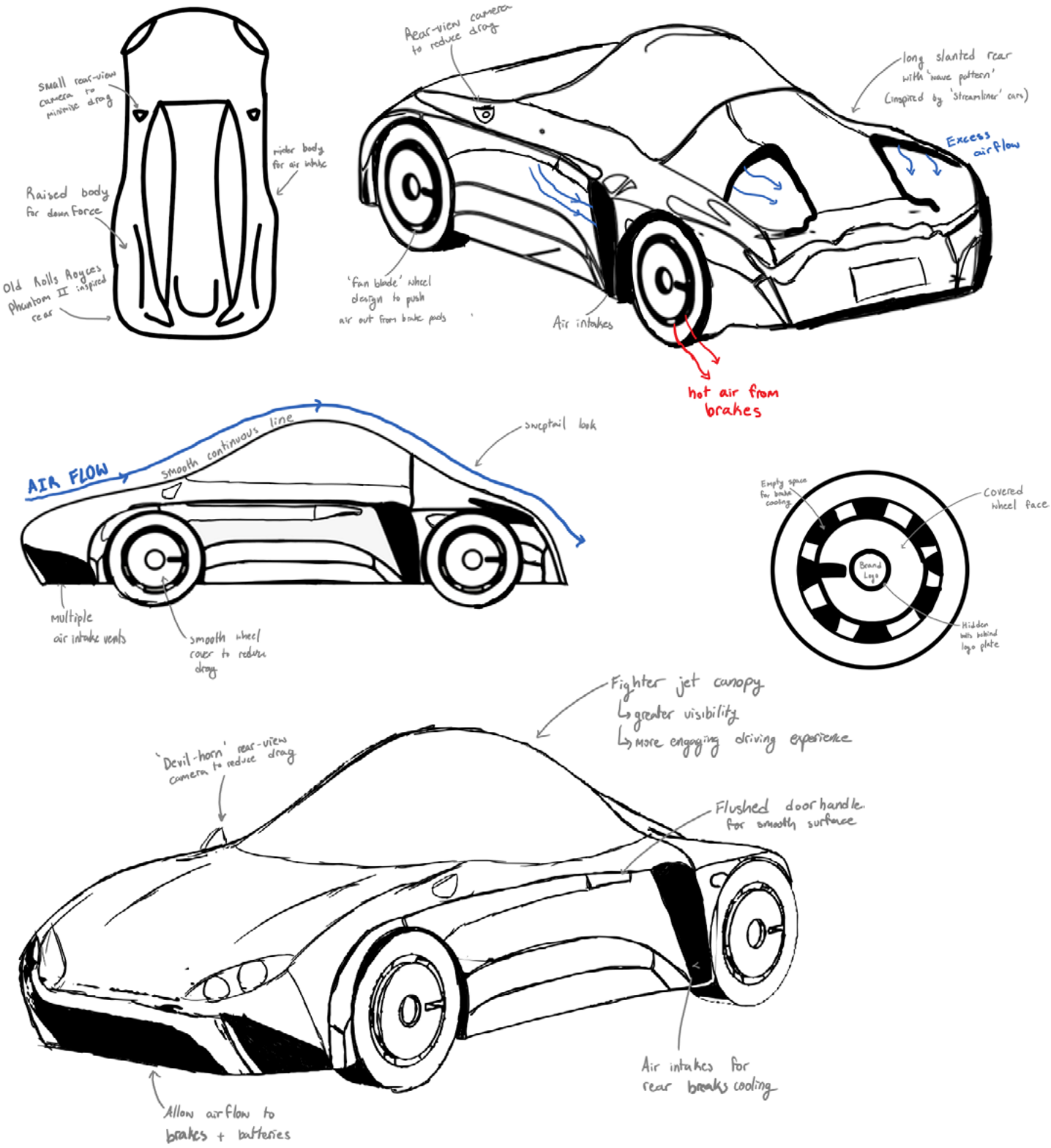

Concept Sketches

Drawing inspirations from classic 1930s style coaches and modern roadster car design, number of sketches were drawn to illustrate the concept design. The concept is characterised by the design fusion between classic luxury coach and roadster layout while maintaining comfort and power of sedans. Having taller passenger cabins than contemporary high performance cars increase usability in daily life.

CAD Designs

[I]

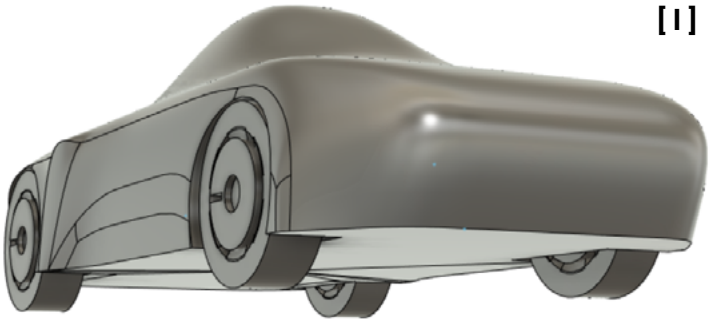

Chassis View	[I]
Front Wheel Close-up	[II]
Side-view (left)	[III]
Top-view	[IV]
Rear-view	[V]
Front-view	[VI]

[II]

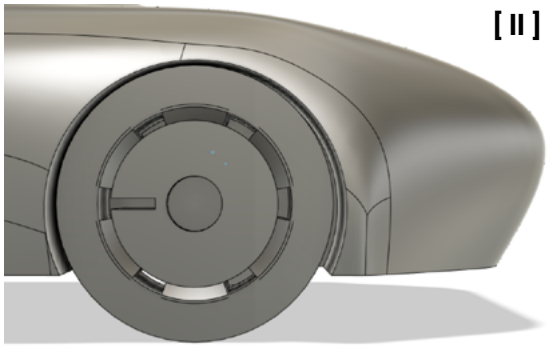

[III]

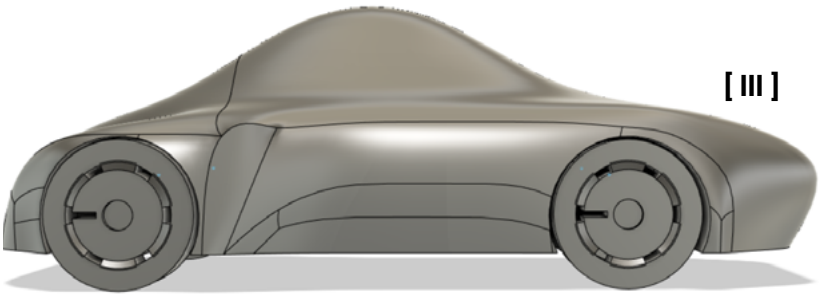

[IV]

[V]

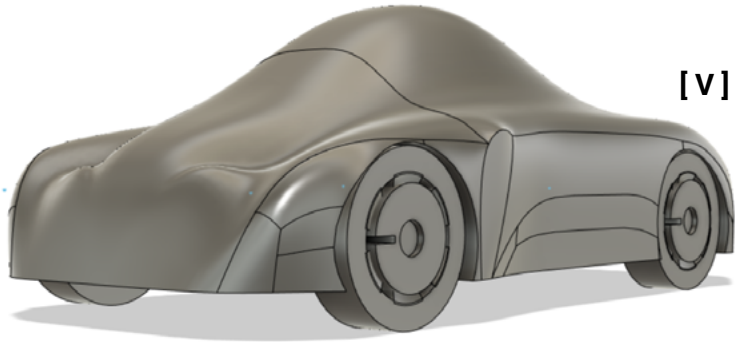

[VI]

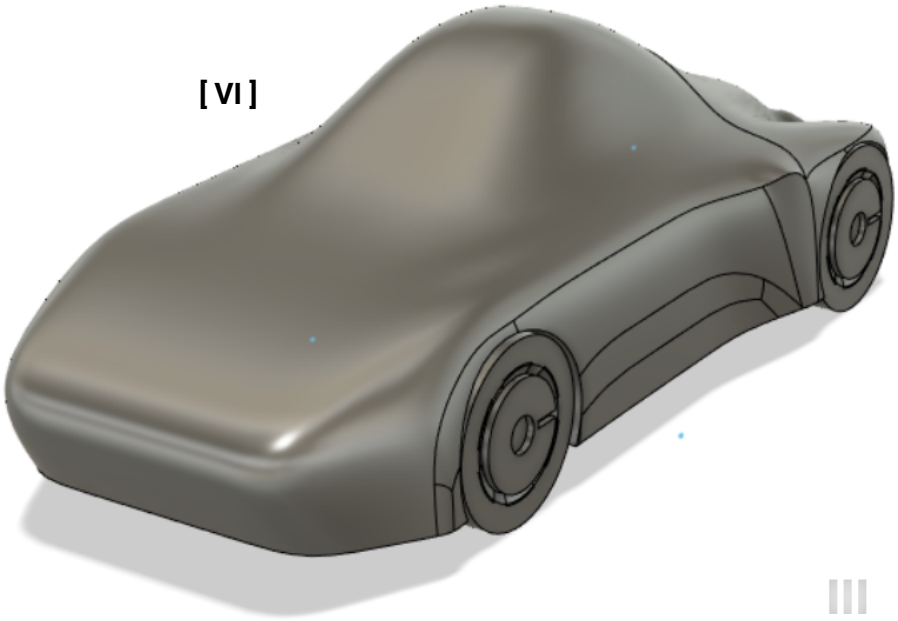

CFD Analysis Summary

Mesh Analysis	
Total Cell Count	914018
Fluid Cells	914018
Solid Cells	247938
Trimmed Cells:	0

Table 1: Mesh Analysis Settings

Additional Physical Calculation Options	
Heat Transfer Analysis (Solid Conduction)	off
Flow Type	Laminar & Turbulent
Time-Dependent Analysis	off
Gravity	-9.81 ms^{-2}
Radiation	off
Humidity	off
Default Wall Roughness	0 µm

Table 2: Additional Physics Settings

Analysis Time	
Calculation Time (CPU)	21695 s
Number of Iterations	777
Warnings	-

Table 3: Analysis Time taken

Material Settings		
Fluids	Air	
Initial Conditions		
Thermodynamics Parameters	Static Pressure	101325 Pa
	Temperature	293.20 K
Velocity Parameters	Velocity Vector	120 km/h
	Velocity (X-Axis)	0 km/h
	Velocity (Y-Axis)	120 km/h
	Velocity (Z-Axis)	0 km/h
Turbulence Parameters	Intensity	0.10%
	Length	0.002 m

Table 4: Environmental Settings

Type	Global Goal
Velocity	
Goal Type	Force (Y-Axis)
Calculate	Average Value
Coordinate System	Global Coordinate System
Use in Convergence	on
Lift Force	
Goal Type	Force (Y-Axis)
Coordinate System	Global Coordinate System
Use in Convergence	on
Drag Force	
Goal Type	Force (Z-Axis)
Coordinate System	Global Coordinate System
Use in Convergence	on
Drag Coefficient Equation	
Formula	(2*Drag force)/(1.225*0.011355*(Velocity)^2)*(-1)
Dimensionality	No units
Use in Convergence	on

Table 5: CFD Global Goal Settings

Results						
Name	Unit	Value	Progress	Criteria	Delta	Use in Convergence
Av Velocity	km/s	118.862	100	0.006	0.010	yes
Lift Force	N	870.003	100	58.007	58.007	yes
Drag Force	N	536.802	100	9.019	5.026	yes
C_D	n/a	0.426	100	1.62E-04	3.99E-03	yes

Table 6: CFD Results

To validate the CFD results, calculations for drag coefficient is solved by hand by categorising different car components into archetypes with known coefficient of drag before plugging into the drag formula. From the lookup table (**Appendix A**), the concept design have the following characteristics: **A-2, B-1, C-1, D-3, E-3, F-1, G-6, H-1**.

Calculations:

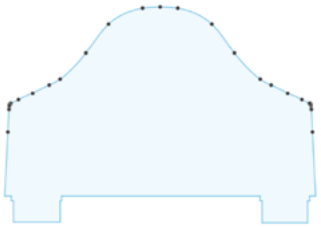

Cross Sectional Area

2.428 m^2

$$C_D = 0.16 + 0.0095 \sum_{i=A}^{H} N_i$$

$$C_D = 0.16 + 0.0095(19)$$

$$C_D = 0.3405$$

$$C_D = \frac{F_{Drag}}{\frac{1}{2}\rho U_\infty^2 A}$$

$$F_{Drag} = 551\ N\ (3sf)$$

The estimated drag calculated is 551N compared to 536N value from the CFD. The 2.69% difference is small enough for the CFD analysis to be validated. The next step is to compare the results with existing archetype after analysing numerical data from the CFD.

$$P = F_{Drag} \times v$$

$$P = 551N \times 33.778ms^{-1}$$

$$P = 18{,}600\ W\ (3sf)$$

Velocity Distribution

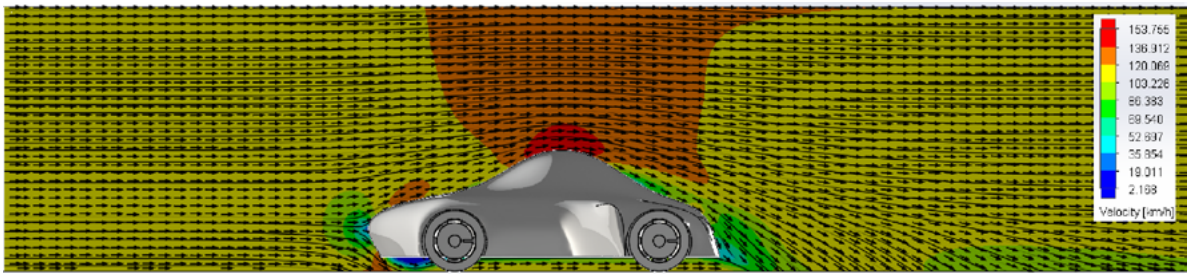

Figure 1: Velocity Distribution (centre cross-section)

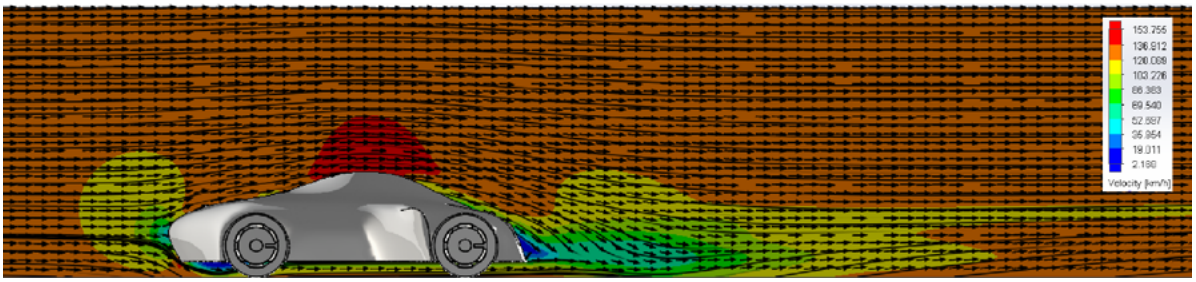

Figure 2: Velocity Distribution (1/4th from centre cross section)

From the CFD analysis, it is noted that when travelling at 120 km/h, the airflow velocity ranges from 2.168 to 153.7 km/h, where the speed is lower at the front, the rear, and the undercarriage. When comparing the 2 figures, it can be observed that there are substantial flow separation at the rear from the centre area of the car is greater than that other cross-section due to the more dramatic change in bumper angle at the centre.

Pressure Distribution

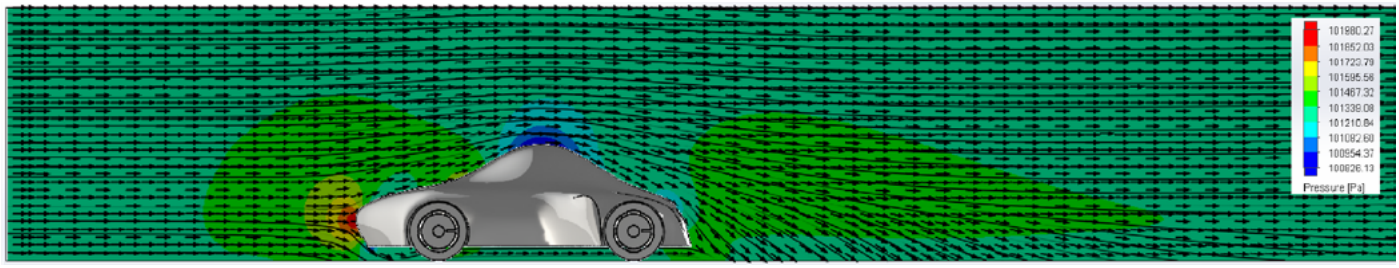

Figure 3: Pressure Distribution (centre cross section)

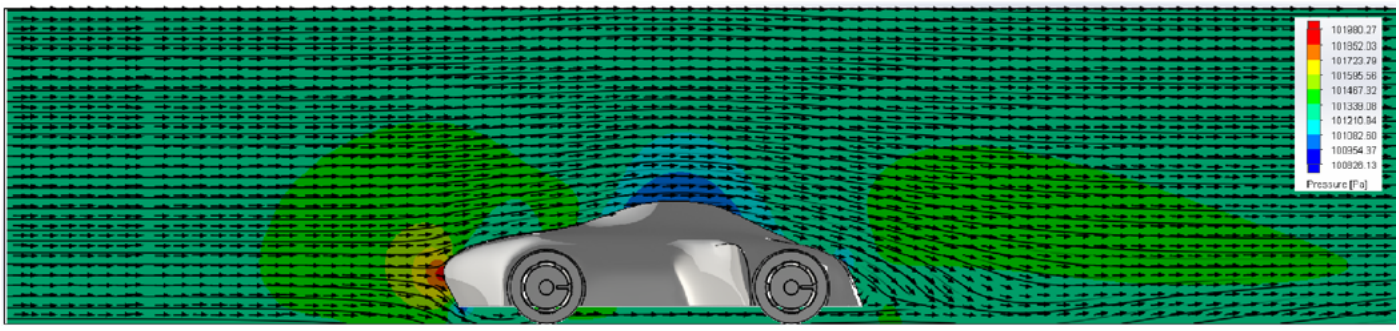

Figure 4: Pressure Distribution (1/4th from centre cross section)

It can be seen that air pressure ranges from 100826 to 101980 Pa, where areas with greater pressure is the same area with lower flow velocity, illustrating Bernoulli's Principle.

Pressure Surface Distribution

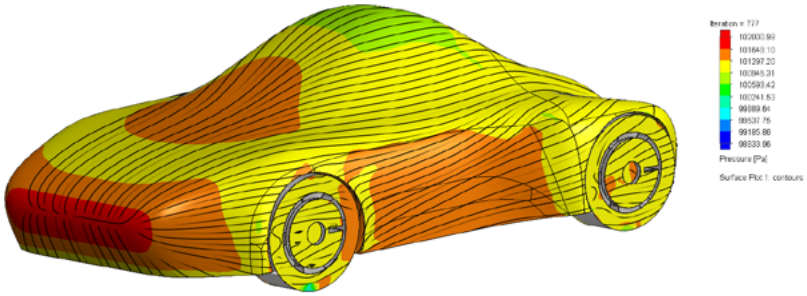

Figure 5: Pressure Surface Distribution Perspective (Front-view)

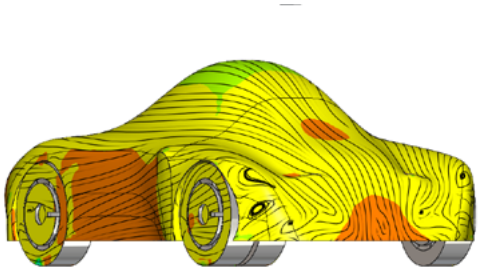

Figure 6: Pressure Surface Distribution Perspective (Rear-view)

Firstly, it should be noted that no pressure surface distribution analysis is made on the wheel tires due to how the point of contact between the rubber and the ground have significantly lower pressure value compared to other sections making it difficult to illustrate difference in pressure in other areas.

Figure 5 shows that the air pressure is greatest at the leading edges in front of the car and the windscreen. This is expected as the leading edges is the first point of contact between the car body and the airflow. As for the windscreen, the reason for greater pressure could be due to the large angle difference between the hood and the glass.

Figure 6 shows the decrease in pressure at the highest point of the passenger compartment and at the tail of the vehicle, suggesting flow separation. The difference is especially clear at the area near the edge between the wheel and the body where the inward curve from the roof to the rear bumper reduce airflow to be channelled to said area.

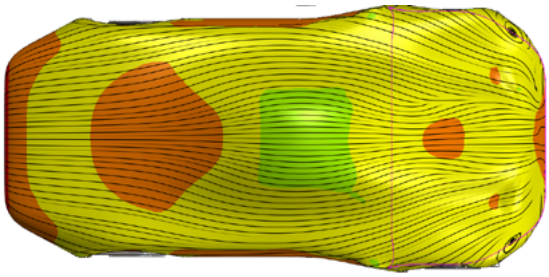

Figure 7: Pressure Surface Distribution top view

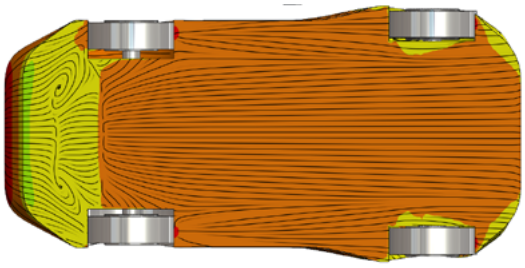

Figure 8: Pressure Surface Distribution undercarriage view

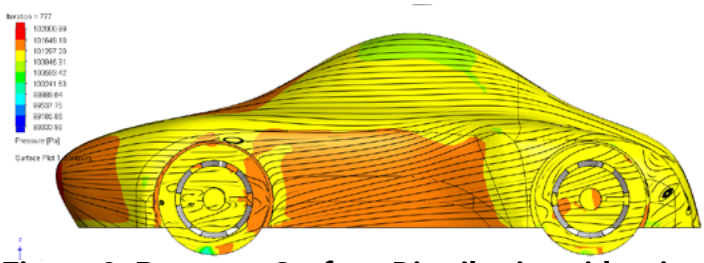

Figure 9: Pressure Surface Distribution side view

Figure 7 shows how raised sections of the rear body panel experiences greater pressure, increasing downforce, and increasing drag.

Figure 8 shows high pressure at the front section of the rear wheels. This is due to the incoming airflow hitting the wheel and moving into the empty cavity of the inner fender.

Isosurface Distribution

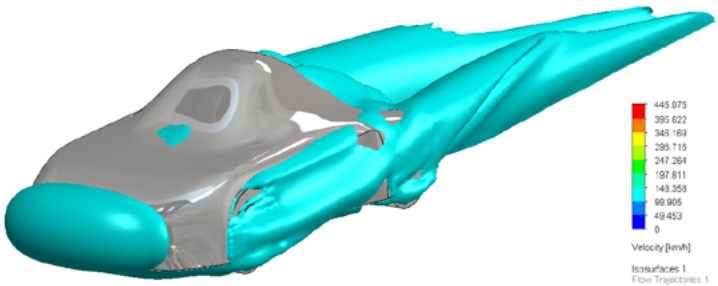

Figure 10: Isosurface Distribution Perspective (Front-view)

Figure 11: Isosurface Distribution side-view

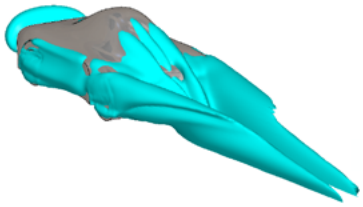

Figure 12: Isosurface Distribution Perspective (Rear-view)

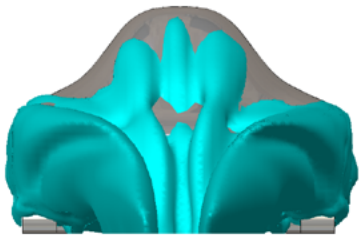

Figure 13: Isosurface Distribution rear-view

3D Flow Trajectory

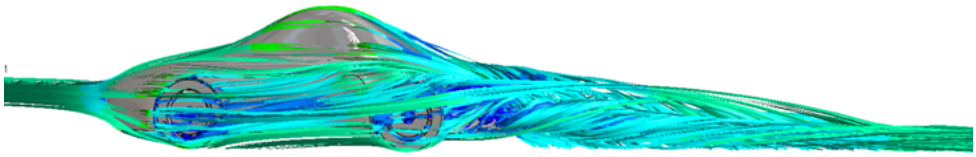

Figure 14: 3D Flow trajectories side-view

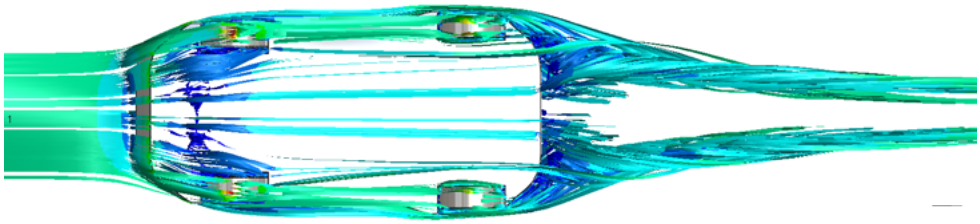

Figure 15: 3D Flow trajectories undercarriage view

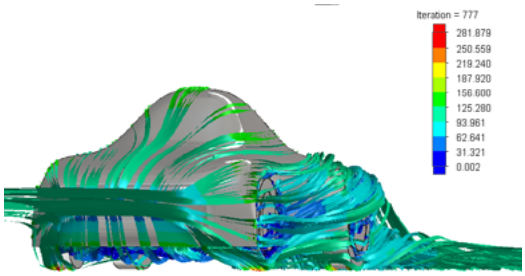

Figure 16: 3D flow trajectories perspective (Front-view)

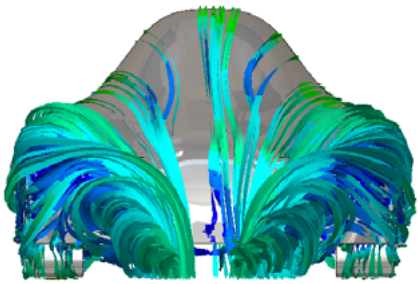

Figure 17: 3D flow trajectories rear-view

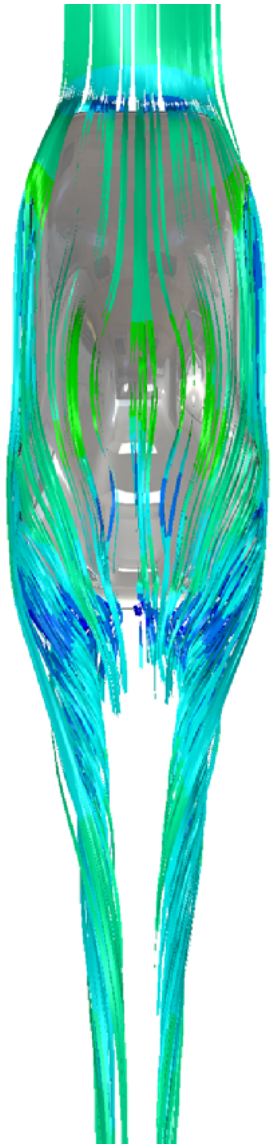

Figure 18: Isosurface Distribution top-view

It can be observed that there are significant eddy currents being generated at the rear due to the shape of the rear panel curving towards the centre, resulting in turbulence and greater pressure drag. This is apparent in **figure 14** where slower airflow from the undercarriage diffused into the faster moving airflow from the upper body panel of the car to counteract the pressure gradient, producing large vortices as shown in **figure 17**.

It is also noted that embossed wheel surface causes air to be trapped, slightly increasing drag.

CFD & Wind Tunnel Review

While both CFD and wind tunnel provide relatively reliable results there are discrepancies between the two as numerical methods (currently) cannot perfectly replicate real environment mainly due to uncontrollable testing environment. This review aims to compare the two methods in-order to find a reliable method in estimating a vehicle's aerodynamic characteristics.

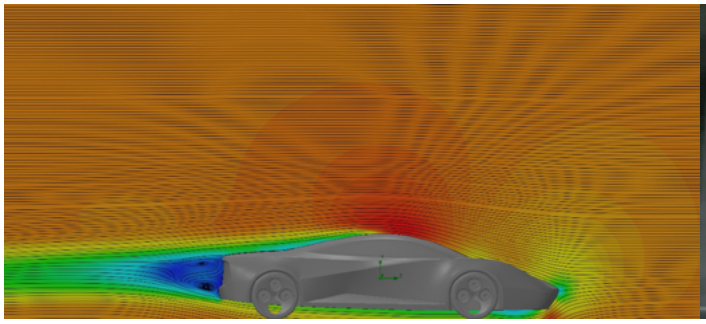

Figure 19: Archetype CFD Analysis

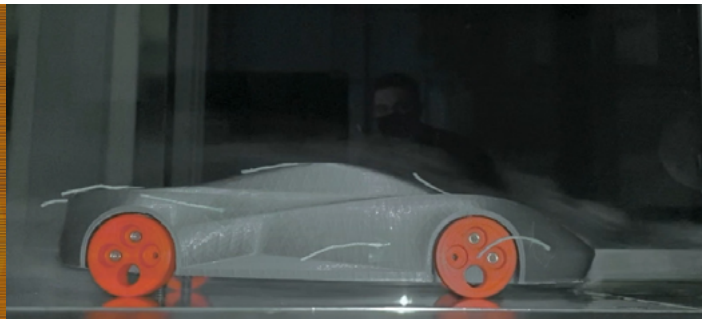

Figure 20: Archetype Wind Tunnel Test

Results				
Name	Unit	CFD	Wind Tunnel	Difference
Velocity	ms^{-1}	30.833	30.552	0.916
Drag Force	N	0.966	1.316	30.675
Lift	N	0.983	-	-
Drag Coefficient	n/a	0.271886	0.37	30.571

Table 7: CFD & Wind Tunnel Results

Drag Force

The most obvious discrepancy between CFD and wind tunnel is the drag force, where the real model experience 36.2% more drag than the CFD model, with strings (used to observe airflow) being one of many reasons. As CFD model does not require drag-inducing strings and runs approximations for Navier-Stokes equations (resulting in more laminar airflow), the drag force is lower than that of the wind tunnel. Furthermore, the CFD analysis is not impacted by the enclosed testing environment of the wind tunnel, meaning the air flow is less turbulent and therefore experience less drag compared to the wind tunnel model.

Velocity

Another contrasting difference between the two experimental methods is the difference in average fluid velocity. As the testing vehicle and the CFD model have the same dimensions the discrepancy is less likely to be caused by the difference in fluid interactions and more likely to cause by the imperfection in the 3D printed model manufacturing process. However as the difference is small this could also be attributed to experimental uncertainty.

Drag Coefficient

As drag coefficient is proportional to *Drag Force over Velocity*, the percentage difference between the two model is the sum of the difference.

Lift

Observations for lift was not made in the wind tunnel test, meaning no comparison can be made between the two experimental methods.

Concept & Archetype Comparison

Results				
Name	Unit	Concept	Archetype	
			CFD	Wind Tunnel
Velocity	ms^{-1}	32.778	30.833	30.552
Drag Force	N	536	0.966	1.316
Lift	N	870	0.983	-
Drag Coefficient	n/a	0.426	0.271886	0.37

Table 8: Concept and Archetype Comparison

While the archetype and the concept dimension is wildly different, it is possible to compare the two using the drag coefficient. From **table 8**, it can be seen that the concept design's drag coefficient is much greater than that of the sports car archetype, having greater commonality with the SUV archetype's values.

Causes of difference in values

Size differences

With the archetype frontal area being 26.8% smaller than that of the concept while having 36.6% lower drag coefficient, it become clears that the biggest source in drag coefficient difference would be the bigger passenger cabin of the concept design. While bigger vehicle size often relates to greater driver comfort and storage space, the increase in surface area in contact with airflow results in greater drag. To overcome this, the improved design should consider having lower vehicle height and incorporating smoother sweeping frontal panel.

Sweptail Rear Panel

With the shape of rear panel rotating towards the centre of the vehicle causing the incoming airflow to form vortices, the vortices reduces the air pressure along the rear edge, resulting in greater pressure drag. In comparison, the shape of the archetype rear have less sharp edges, particularly at the edge between the undercarriage and the rear bumper, meaning there is less flow separation, reducing vortices and pressure drag.

Archetype	Coefficient of Drag	
	CFD	Wind Tunnel
Sports Car	0.27	0.37
Sedan	0.28	0.37
Pickup	0.44	0.52
SUV	0.43	0.43

Table 9: Archetype Coefficient of Drag

Concept Wind Tunnel Predictions

Assuming that the percentage difference for drag coefficient between the CFD and Wind tunnel experiment is constant at 30.6%, it can be predicted that the concept design's experimental drag coefficient would be 0.556, too high for a typical sports car.

Regardless, due to the fact that the archetype model is not to scale unlike the concept CAD, it is difficult to judge the accuracy of any analysis (both CFD and Wind Tunnel) with certainty as fluids do behave differently depending on the scale, velocity, and other environmental factors. Therefore, the next step to produce a more reliable comparison would be to run the experiment on the true scale version of the archetype.

Design Improvements

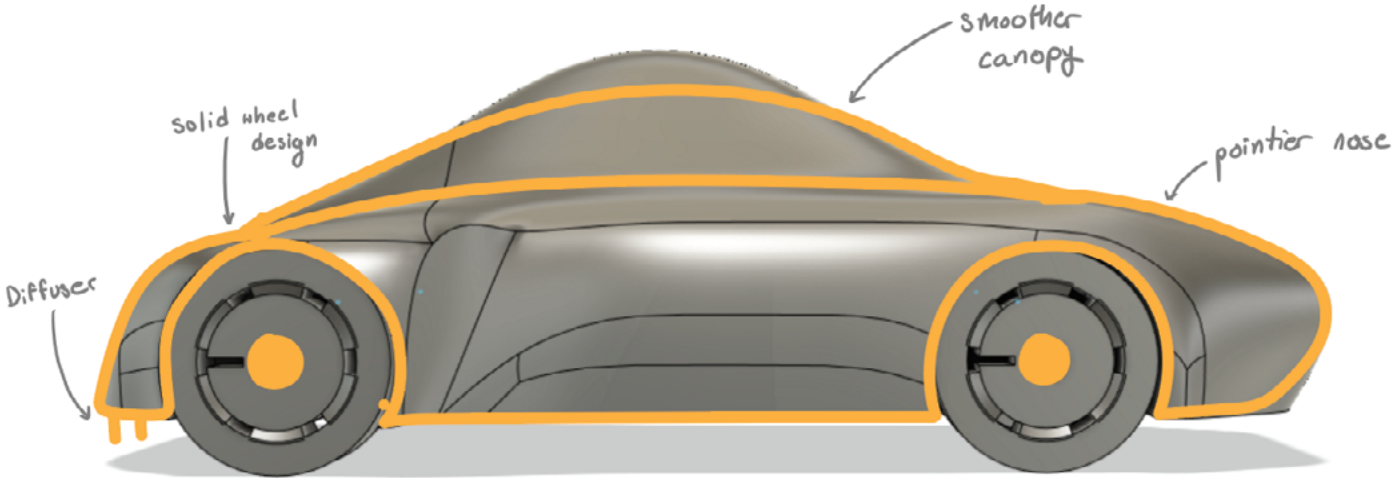

Figure: Improved Concept Side-view

Pressure Reduction
The sharp nose of the car is refined with rounded edges while the canopy angle is reduced, both to reduce the pressure on the car surface.

Sharp Edges Reduction
The sharp edges of the fender and the rear bumper is smoothened to reduce flow separation.

Rear Diffuser
Rear diffuser is added to reduce turbulence from airflow under the car. This works by reducing the airflow pressure, resulting in increased velocity, allowing said airflow to gradually diffused into the higher pressure ambient airflow

Downforce Expansion
Being a high-performance car, the raised rear body would increase down force, improving the vehicle's performance in turns. While this would increase drag, further geometry refinement can ensure net positive performance from this design choice.

Smoother Wheel Surface
As wheel coverage area is inversely proportional to drag coefficient, by increasing the coverage area we can reduce drag. Additionally, the greater coverage reduce airflow that would feed the jetting vortex, further reducing pressure drag.

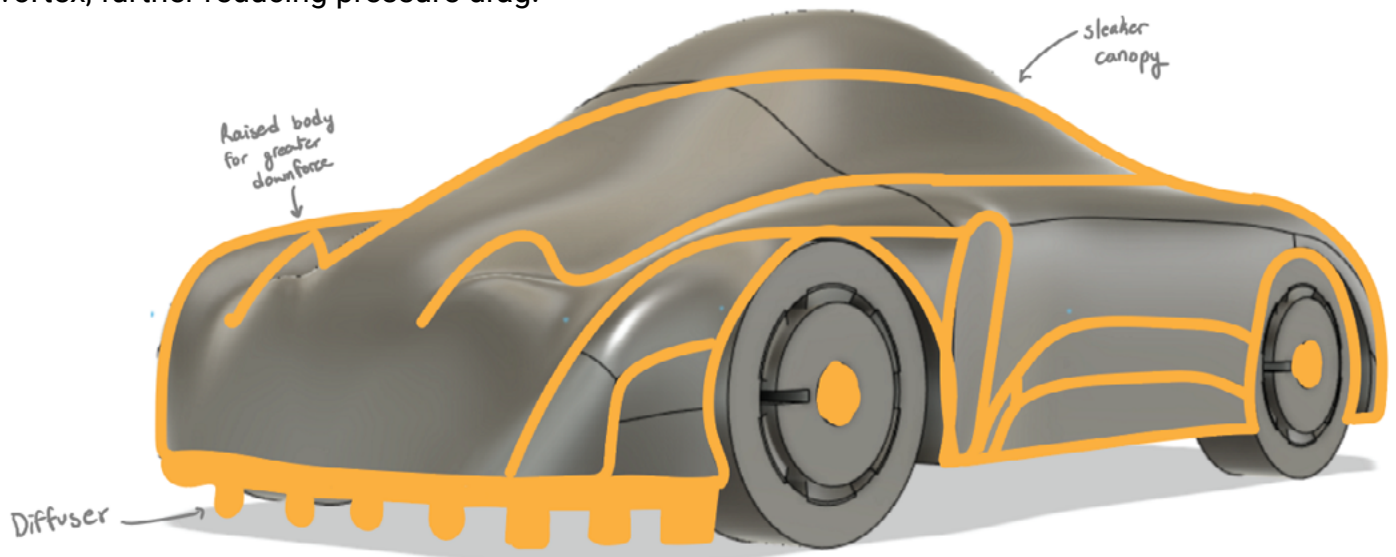

Figure: Improved Concept Perspective (Rear-view)

Appendix

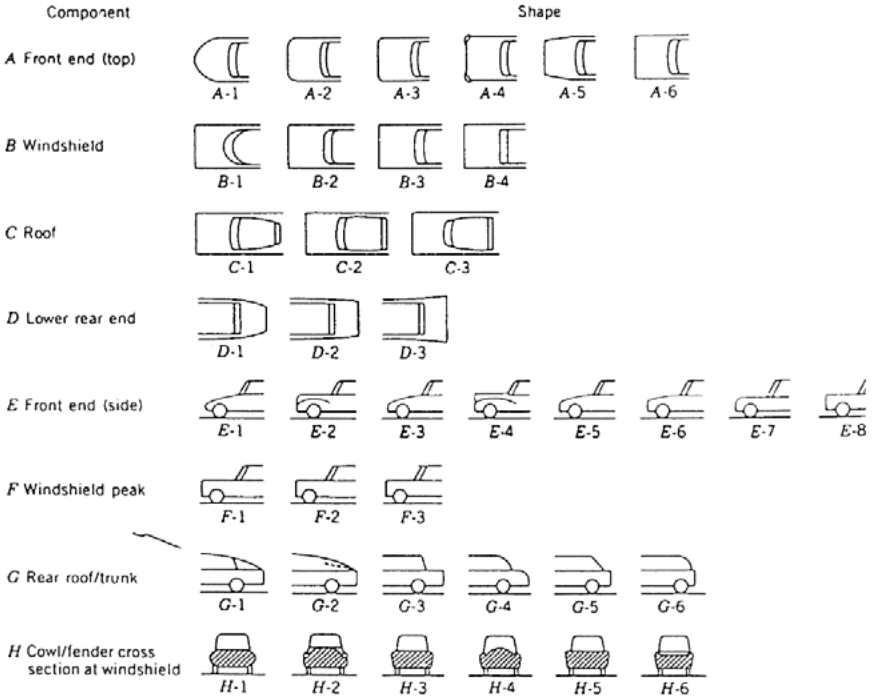

Appendix A: Characteristics of Automobile Components

A. Plan view, front end			
N_A =	1	A-1	Approximately circular
	2	A-2	Well rounded outer quarters
	3	A-3	Rounded corners without protuberances
	4	A-4	Rounded corners with protuberances
	5	A-5	Squared tapering in corners
	6	A-6	Squared constant width front
B. Plan view, windshield			
N_B =	1	B-1	Full wraparound (approximately semi-circular)
	2	B-2	Wraparound ends
	3	B-3	Bowed
	4	B-4	Flat
C. Plan view, roof			
N_C=	1	C-1	Well or medium tapered to rear
	2	C-2	Tapering to front and rear or approximately constant width
	3	C-3	Tapering to front (maximum width at rear)
D. Plan view, lower rear end			
N_D=	1	D-1	Well to medium tapered to rear
	2	D-2	Small taper to rear or constant width
	3	D-3	Outward taper (or flared out fins)
E. Side elevation, front end			
N_E=	1	E-1	Low rounded front, sloping up
	1	E-2	High tapered rounded hood
	2	E-3	Low, squared front, sloping up
	2	E-4	High tapered squared hood
	3	E-5	Medium height, rounded front, sloping up
	4	E-6	Medium height, squared front, sloping up
	4	E-7	High, rounded front, with horizontal hood
	5	E-8	High squared front, with horizontal hood
F. Side elevation, windshield peak			
N_F=	1	F-1	Rounded
	2	F-2	Squared (including flanges or gutters)
	3	F-3	Forward projecting peak
G. Side elevation, rear roof/trunk			
N_G=	1	G-1	Fastback (roofline continuous to tail)
	2	G-2	Semi-fastback (with discontinuity in line to tail)
	3	G-3	Squared roof with trunk rear edged squared
	4	G-4	Rounded roof with rounded trunk
	4	G-5	Squared roof with short or no trunk
	5	G-6	Rounded roof with short or no trunk
H. Front elevation, cowl and fender cross section at windshield			
N_H=	1	H-1	Flush hood and fenders, well rounded body sides
	2	H-2	High cowl, low fenders
	3	H-3	Hood flush with rounded top fenders
	3	H-4	Hood flush with square edged fenders
	4	H-5	Hood flush with square edged fenders
	5	H-6	Depressed hood with high square edged fenders

Appendix B: N_A values of Automobile Components

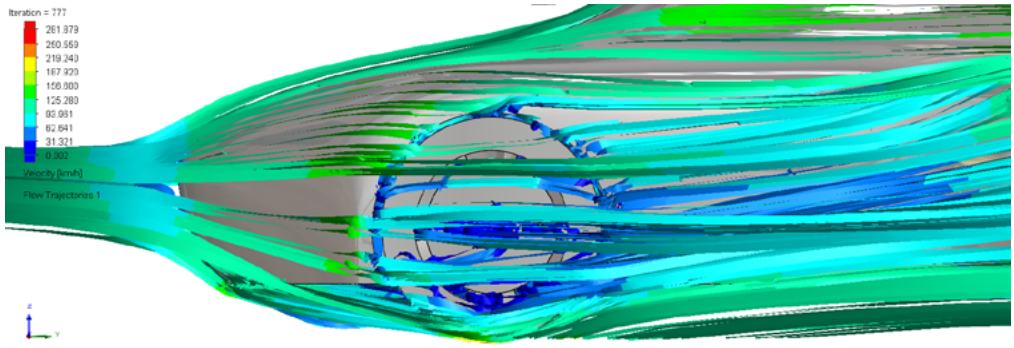

Appendix C: 3D flow trajectory at the front wheel

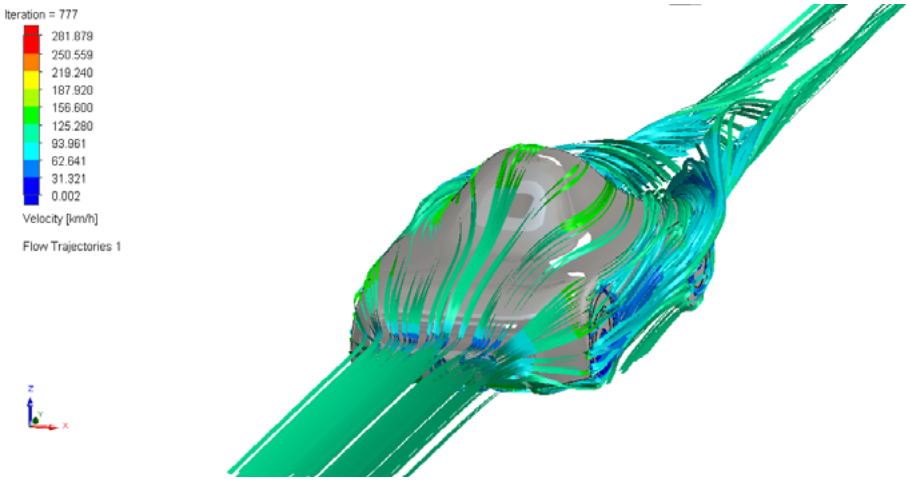

Appendix D: 3D flow trajectory perspective (front/top-view)

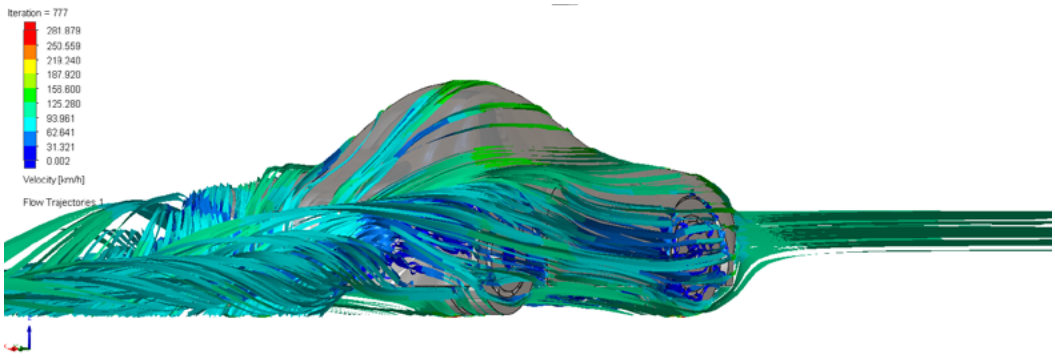

Appendix E: 3D flow trajectory perspective (rear-view)

References

[1] Brandt, A., Berg, H., Bolzon, M., & Josefsson, L. (2019). The effects of wheel design on the aerodynamic drag of passenger vehicles. SAE Technical Paper Series. https://doi.org/10.4271/2019-01-0662
[2] White, R. G. (1969). A method of estimating automobile drag coefficients. SAE Technical Paper Series. https://doi.org/10.4271/690189

Thermofluids: Energy & Design

Vehicle Design Aerodynamics

Beam Suwiwatchai